Robustness of Fourier Ptychographic Imaging to Variation of System Parameters

Moritz Siegel; Austrian Institute of Technology (AIT) & Technische Universität (TU Wien); Vienna, Austria: Lukas Traxler; Austrian Institute of Technology (AIT); Vienna, Austria: Laurin Ginner; Austrian Institute of Technology (AIT); Vienna, Austria

Abstract

In most optic systems images are captured using a CCD/CMOS sensor, where the phases of the converted photons are inevitably lost. Fourier Ptychographic Microscopy (FPM) circumvents this issue by capturing normal microscopy images, and Fourier transforming them computationally (hence the name). Reconstructing the complex object not only yields amplitude but also phase information, enhanced up to super-resolution. Yet one disadvantage remains unsolved: FPM is a very ill-posed problem, the algorithm is not guaranteed to converge to the correct solution, if it converges at all. In practice this means that there is reasonable doubt if the recovered image actually represents the object under the microscope. This work inquires the quality of FPM reconstruction under variation of important system parameters in simulation and experiment. It shows that the alignment of the illumination source is quite critical: even 0.2 degrees off renders reconstruction useless. This paper thus furthers the cost-benefit analysis of which amount of computation time should be spent on digital post-correction.

Fourier Ptychographic Microscopy

Fourier Ptychographic Microscopy (FPM) is a computational imaging technique trading multiple images coherently illuminated from different angles and computation time for a high resolution complex image. Measuring the phase of a light-field is non-trivial and usually quite complicated; comprising of lasers for coherent light creating diffraction patterns, which need special detectors with large dynamical range. FPM circumvents this problem by capturing generic microscopic images (in real space), and transforming them computationally into Fourier space—hence the name. Now one can utilise standard phase retrieval techniques dating back to the eighties [3], to combine the images to a synthetic aperture. Which yields a recovered image, not only of a resolution orders of magnitude higher than the images on their own; it even overcomes the resolution limit of the optical system, obtaining super-resolution [5]. Additionally, the final image is a complex object, it not only contains amplitude-, but phase information as well. This enables FPM to work on translucent objects, like biological samples, without the need of staining. Various work has been done on using FPM on translucent objects (e.g. cells), multi-colour-reconstruction [5], digital refocusing [5], high-speed high-throughput video [6]. Yet one disadvantage remains: The Gerchberg–Saxton (GS) algorithm [4], which is a type of gradient descent (the formulation is often non-convex), is not guaranteed to converge to the correct solution (the global minimum) [8]. Relying solely on low resolution amplitude images as ground truth—the phase generally being unknown—assigning reconstruction quality is non-trivial. In practice this means that

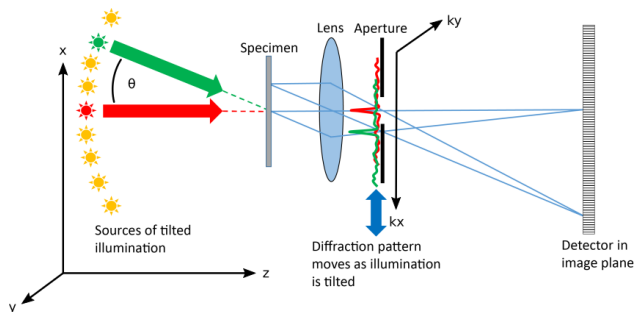there is reasonable doubt if the recovered image actually represents the object under the microscope.

*Figure 1: Schematic concept of the microscope for FPM, 3D illumination source position **r** and 2D Fourier space locations **k**, adapted from [7].*

A schematic illustration of a typical FPM setup is shown in Figure 1; θ angle-varied illumination source (left) illuminates a target, which results in a diffraction pattern at the aperture. The detector is at focus, and so captures generic images.

To put FPM recovery in a nutshell, we show the full procedure in Algorithm 1. In the following description we refer to the corresponding lines in brackets.

The core of FPM is an iterative outer loop, in which an inner loop is covering the images ι_n from all n different incident illumination wave-vectors $\mathbf{k}_n$ (angle θ_n) sequentially (lines 2–10); until the FPM algorithm can be considered converged after ℓ outer loops. Convergence is estimated by the pixel-wise Root Mean Square (RMS) Error E_ℓ, the deviation of the current high-resolution spectrum $\hat{O}_\ell$ to the last iteration's $\hat{O}_{\ell-1}$ (line 10). For all n low resolution amplitudes $a_n = \sqrt{\iota_n}$, in each of these ℓ loops; the part of the high-resolution (indicated by upper case letters) complex object's spectrum $\hat{O}$, corresponding to the incident illumination $\mathbf{k}_n$, is rescaled to low-resolution (lower case letters) size $(\eta/\zeta)^2$ and convolved with the pupil function $\hat{P}$ of the optical system (line 5). The resulting low-resolution spectrum $\hat{o}_n$ is now inverse Fourier transformed to o_n (line 6), and its phase ϕ_n is computed (line 7). The estimation $\ell+1$ is now given by the combination of the amplitude of the measured image a_n and the phase of the corresponding recovered object o_n (line 8). In the next step, the high-resolution spectrum $\hat{O}$ gets updated with the Fourier transform $\hat{o}_n$ of that new estimation o_n (line 9). Reaching convergence, the resulting spectrum $\hat{O}$ finally is inverse Fourier transformed, yielding the high-resolution complex object O (line 11); And thus amplitude $A = |O|$ and phase $\Phi = \angle O$.

An exemplary FPM recovery is shown in Figure 2; spectrum (2b), amplitude (2c) and phase (2d), where one can clearly see the

Algorithm 1 Fourier Ptychography Core

1: **function** REKOVER(a)
2:     **while** $E_\ell > \varepsilon$ **do**
3:         $\ell \leftarrow \ell + 1$
4:         **for all** $\mathbf{k}_n$ **do**
5:             $\hat{o}_n \leftarrow (\frac{\zeta}{\eta})^2 \hat{O}_{\mathbf{k}-\mathbf{k}_n} * \hat{P}$
6:             $o_n \leftarrow \mathscr{F}^{-1}(\hat{o}_n)$
7:             $\phi_n \leftarrow \angle o_n$
8:             $o_n \leftarrow a_n e^{\mathbf{i}\phi_n}$
9:             $\hat{O}_{\mathbf{k}-\mathbf{k}_n} \leftarrow (\frac{\eta}{\zeta})^2 \mathscr{F}(o_n) * \hat{P}$
10:         $E_\ell \leftarrow \sqrt{<|\hat{O}_\ell - \hat{O}_{\ell-1}|^2>}$
11:         $O \leftarrow \mathscr{F}^{-1}(\hat{O}_\ell)$

improved resolution compared to the best single low-resolution image (2a).

(a) Low-resolution Amplitude   *(b) Recovered Spectrum*

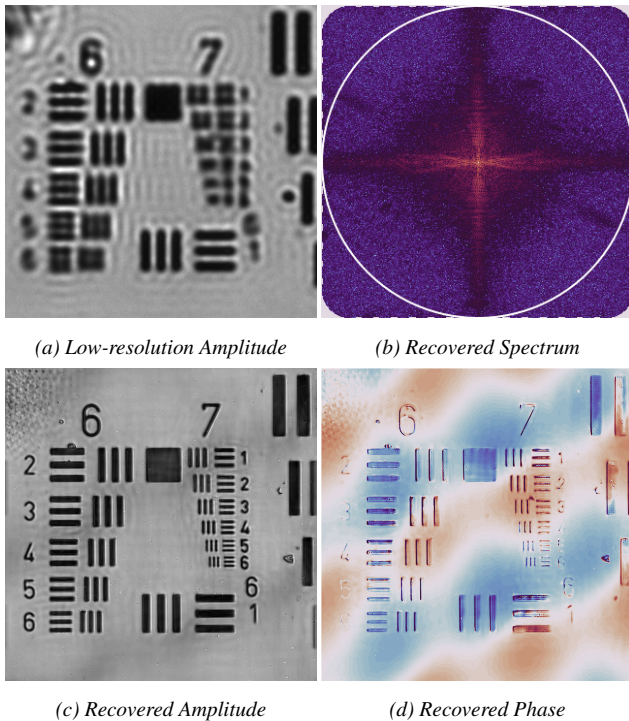*(c) Recovered Amplitude*   *(d) Recovered Phase*

Figure 2: Examples from the FPM process; The central (best) low resolution image 2a, recovered high-resolution spectrum 2b, amplitude 2c and phase 2d.

Alignment Simulations

The scope of this work is to investigate the robustness of FPM to variation of the critical system parameters. Based on the GS algorithm, FPM uses multiple images taken from different illumination angles, so recovery obviously relies on the knowledge of the illumination positions, but to what degree? The objective of this paper is to investigate the six degrees of freedom of the illumination setup for its respective impact on the subsequent FPM recovery.

The most convenient and frequently used setup for the illumination is a shift- register controlled RGB LED matrix, made for displays in urban spaces. This makes it a cheap and easy to implement solution proven to work [5], in spite of not all the LEDs being equidistant to the target.

Simulating FPM recovery is quite a straight forward task, as the concept is basically embedded in the FPM algorithm itself. The procedure of this simulation is shown in Algorithm 2, which closely follows the nomenclature from Algorithm 1: Multiple images are rendered as if from various illumination angles $\mathbf{k}_n$, and so comprise different regimes in spatial frequency space of the complex object. So if one happened to know the complex object (amplitude and phase) beforehand (line 2), its Fourier transform could be decomposed into a stack of simulated low-resolution amplitudes a_n (lines 7–8)! These stacks are generated step wise (line 4) with respect to the system parameter of interest x_m e.g. shift in x-axis (line 5), each time recovered using the standard FPM algorithm (line 9).

Quite on the contrary to actual experiments, in simulations like this, we are able to readily denote the quality of the reconstruction: Every step during recovery, we can compare the complex object with the ground truth, summing over the root mean square error (RMSE) of the differences.

Algorithm 2 Alignment Simulation

1: **procedure** ALIGNING(A, Φ, m)
2:     $O \leftarrow A e^{\mathbf{i}\Phi}$
3:     $\hat{O} \leftarrow \mathscr{F}(O)$
4:     **for all** m misalignments x_m **do**
5:         $\mathbf{k}_n \leftarrow$ KRID($\Delta x, \Delta y, \Delta z, \rho, \psi, \gamma$)
6:         **for all** $\mathbf{k}_n$ **do**
7:             $\hat{o}_n \leftarrow (\frac{\zeta}{\eta})^2 \hat{O}_{\mathbf{k}-\mathbf{k}_n} \hat{P}$
8:             $a_n \leftarrow \mathscr{F}^{-1}(\hat{o}_n)$
9:         $O_m \leftarrow$ REKOVER(a)

The k-space positions $\mathbf{k}_n$ corresponding to the locations $\mathbf{r}_n$ of the physical LEDs in real space are defined according to Algorithm 3: To simulate misalignment of all six degrees of freedom, the LED's positions $\mathbf{r}_n$ are first rotated about the x-,y-, and z-axis (respective rotation matrices R_ρ, R_ψ, R_γ in line 2). The rotated grid $\mathbf{r}$ is then shifted in x-,y-, and z-axis (line 3) and mapped to the two-dimensional sensor plane (line 4) in Fourier space, where $k_0 = 2\pi/\lambda$ denotes the spatial frequency of the incident light.

Algorithm 3 K-space Grid Variation

1: **function** KRID($\Delta x, \Delta y, \Delta z, \rho, \psi, \gamma$)
2:     $\mathbf{r} \leftarrow R_\gamma R_\psi R_\rho \mathbf{r}$
3:     $\mathbf{r} \leftarrow \mathbf{r} + \Delta x + \Delta y + \Delta z$
4:     $\mathbf{k} \leftarrow -k_0 \sin(\arctan(\mathbf{r}_x./\mathbf{r}_z))$

A slightly misaligned LED panel is exemplary shown in Figure 3; the LED panel with 6 mm spaced LEDs is positioned at a height of -80 mm (below the target), with a shift of 1 mm in x-, y-, z-axis, and 1° each tilt, roll, and yaw. The corresponding k-space grid is shown in Figure 4.

Alignment Calibration

A structural downside of FPM is that the illumination source is off-focus, so its alignment is—though crucial—not directly
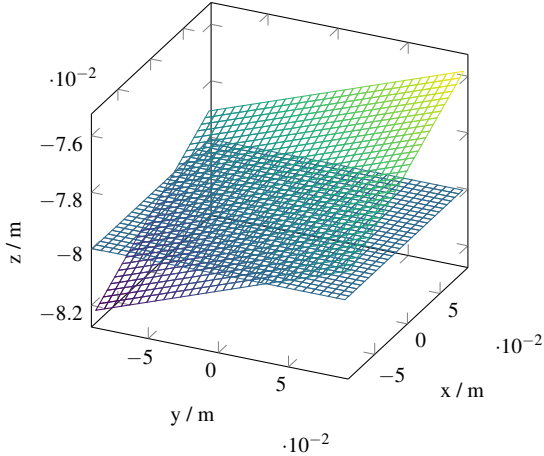
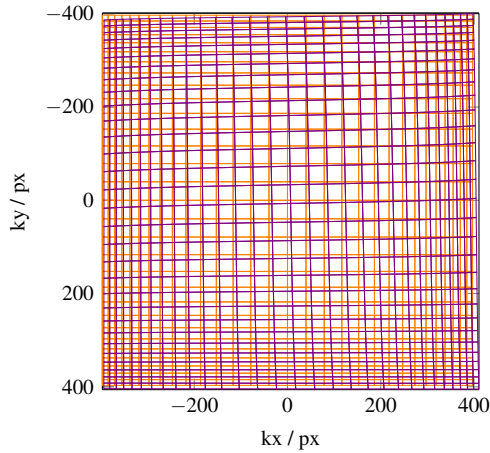*Figure 3: LED positions (nodes) of a slightly misaligned panel in 3d real space.*

Figure 4: Comparison of the k-space projections $\mathbf{k}_n$ (nodes) of the LED positions of a slightly misaligned panel (violet) shown in Figure 3; versus the initial panel (orange).

measurable. Fortunately numerical calibration is still possible, at least for the images taken under bright-field conditions: Via autocorrelation. First proposed by [2], to circumvent the former expensive embedded corrections: A surprisingly simple yet beautiful calibration algorithm using autocorrelation to correct for the positions. As icing on the cake, during the process this method necessarily corrects the magnification of the optical system, which is usually known only to some degree. Based on [2], yet quite contrarily, the proposed method is a standalone calibration: Introducing a single step running prior to, and completely detached of, the standard FPM routine!

In the experimental FPM setup, the camera records intensity images ι_n, where n indicates the illumination direction θ_n of a coherent plane wave which corresponds to the spatial frequency $\mathbf{k}_n$ in the high-resolution spectrum $\hat{O}$. The images two-dimensional Fourier transform $\hat{\imath}_n$ can be related to:

$$\hat{\imath}_n = \mathscr{F}\{\iota_n\} = \mathscr{F}\{|a_n|^2\} = \hat{a}_n \star \hat{a}_n \tag{1}$$

where $\star$ denotes autocorrelation of the amplitude a_n, as a special case of cross-correlation. the Fourier transform $\hat{\imath}_n$ of n-th discretely sampled intensity image captured by the camera can be

modelled according to:

$$\hat{\imath}_n \cong (\hat{P} * \hat{O}_{\mathbf{k}-\mathbf{k}_n}) \star (\hat{P} * \hat{O}_{\mathbf{k}-\mathbf{k}_n}) \tag{2}$$

Typically a Fourier spectrum decays sharply from the DC term—the average (arithmetic mean) of the entire image, located at frequency zero, thus at the centre—toward higher frequencies, usually about a few orders of magnitude. Only when the image ι_n is illuminated under bright field conditions, the DC term of the object spectrum $\hat{O}(\mathbf{k} - \mathbf{k}_n)$ is located within its pupil's pass band $\hat{P}$; leading to high values where the pupil overlaps the DC term, and negligible outside. The position correction problem now shifted to a much simpler image recognition problem! One simply needs to fit two circles to the disks of each of the spectra $\hat{\imath}_n$, to find the illumination positions $\mathbf{k}_n$ and $-\mathbf{k}_n$.

Algorithm 4 Alignment Calibration

1: $\hat{\imath}_n \leftarrow \mathscr{F}\{\iota_n\}$
2: $\hat{\imath}_n \leftarrow |\hat{\imath}_n|/\text{mean}_n(|\hat{\imath}_n|)$
3: $\hat{\imath}_n \leftarrow \log_{10}(\hat{\imath}_n)$
4: $\hat{\imath}_n \leftarrow \text{gauss}(\hat{\imath}_n, \sigma)$
5: **for all** m $\subset$ n images **do**
6: $\quad r_n \leftarrow \text{imfindcircles}(r \pm \Delta r, \; \varepsilon)$
7: $r \leftarrow \text{median}_n(r_n)$
8: **for all** n images **do**
9: $\quad \mathbf{c}_1, \mathbf{c}_2 \leftarrow \text{imfindcircles}(r)$
10: $\quad \mathbf{c}_n \leftarrow \text{argmin}_{1,2}(|\mathbf{c}_{1,2} - \mathbf{k}_n|)$

The alignment calibration procedure proposed by [2] is shown in Algorithm 4, the corresponding lines are shown in brackets: For a set of n low-resolution images ι_n, the two-dimensional Fourier transform is computed. The magnitude of these spectra is divided by their mean, to filter out the sample information, which we are not interested right now (line 2). The Fourier spectra usually span some orders of magnitude, even after the DC term is lost, so we take the logarithm (line 3). Since the following function for the circle detection, `imfindcircles` [1] (part of the `image` package in octave forge) is based on a Hough transform—alas on edge detection—it wants the background as smooth as possible. So we blur the image, where $\sigma = 2$ was found empirically to work well (line 4). Since the Hough transform tests all possible circles, its speed heavily relies on the knowledge of the radii, which are in the case of FPM all the same and based on the cutoff frequency.

So we first run `imfindcircles` on a subset $m \subset n$ with our initial guess for the radius with some reasonable deviation, subsequently taking the median of the n best radii (line 7). Using this estimated radius to initialize the Hough transform, we search for the two best circles in all n images (line 9), since all the low-resolution images contain two autocorrelation discs (at $\mathbf{k}_n$ and $-\mathbf{k}_n$), due to the symmetry of the problem. Based on our initial positions $\mathbf{k}_n$, we take the one nearest of the two $\mathbf{c}_{1,2}$, in order to get all the different positions once (line 10), leaving us with n corrected positions $\mathbf{c}_n$.

This calibration has to be performed only once for a given microscope setup, subsequent FPM recovery operations can all use the corrected bright field positions $\mathbf{c}_n$, as shown exemplary for one experimental setup and three simulations in Figure 5.

Additionally the radius r is linked to the magnification M of the optical system, and so represents a possibility to correct:

$$M = \frac{\text{NA} l_i l_s}{\lambda r} \qquad (3)$$

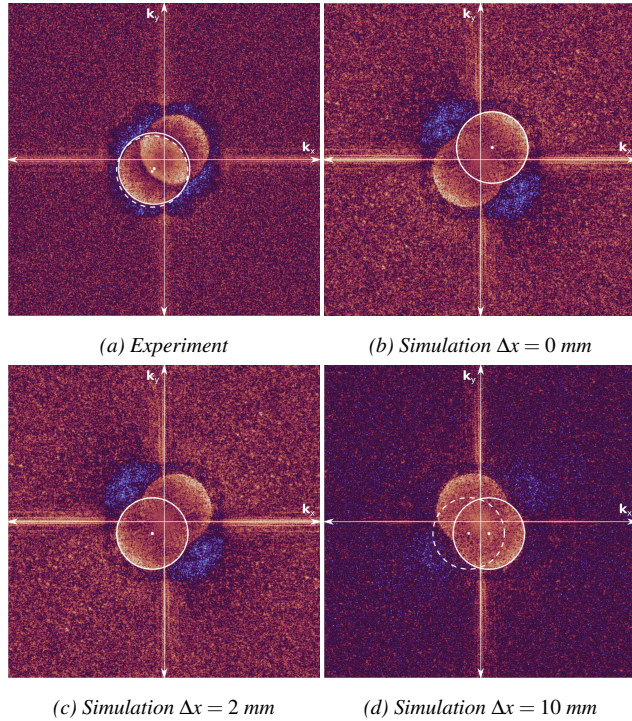where l_i denotes the size of the low-resolution image ι, and l_s the pixel size of the sensor.

(a) Experiment *(b) Simulation $\Delta x = 0$ mm*

(c) Simulation $\Delta x = 2$ mm *(d) Simulation $\Delta x = 10$ mm*

Figure 5: Alignment Correction: Comparison of exemplary spectra $|\hat{\iota}_n|$ (Algorithm 4 line 4) of both experiment (5a) and simulation (5b–5d), for the same arbitrary illumination angle $\theta_n = 1.5°$ at increasing shift; One can clearly see the autocorrelation circles, the corresponding illumination positions and pupil radii are shown for assumed (x, dashed line) and found (o, line).

Alignment Correction

Considering the geometry of FPM it is hardly surprising to see a strong correlation between alignment perfection, and the quality of the obtained result. Interestingly, this work shows on the basis of simulations, that even a misalignment of the illuminating LED matrix of only a 0.2 degrees (equivalent to a shift of 1mm for the used LED matrix' optimal setup) poses a serious threat to FPM recovery! This result is exemplary shown for three different misalignment of the LED panel (shift in x-axis) in Figure 6, using arbitrary images as a basis for amplitude and phase. Interestingly FPM is able to recover the amplitude even under bad conditions, as one can see all of the racoons quite clearly. Unfortunately the recovered phase is heavily distorted even at tiny misalignment of $0.35°$ (2mm shift)! This explains the need for careful calibration and correction algorithms used widely [2].

The main goal here is to find misalignment of the whole LED panel, even though it is conceivable that some individual LEDs are mispositioned on panel assembly level too.

Shift

Since the most common experimental setup for FPM is a LED panel, the most important alignment calibration probably is the shift in x-axis, respective y-axis [2]. The height (shift in z) is comparatively easy to adjust by direct measurement, whereas the shift in x, y, is extremely tedious to measure. This is due to the fact, that the LED panel is off focus, so there is no easy way of answering the question where the centre really is, in respect to the optical path.

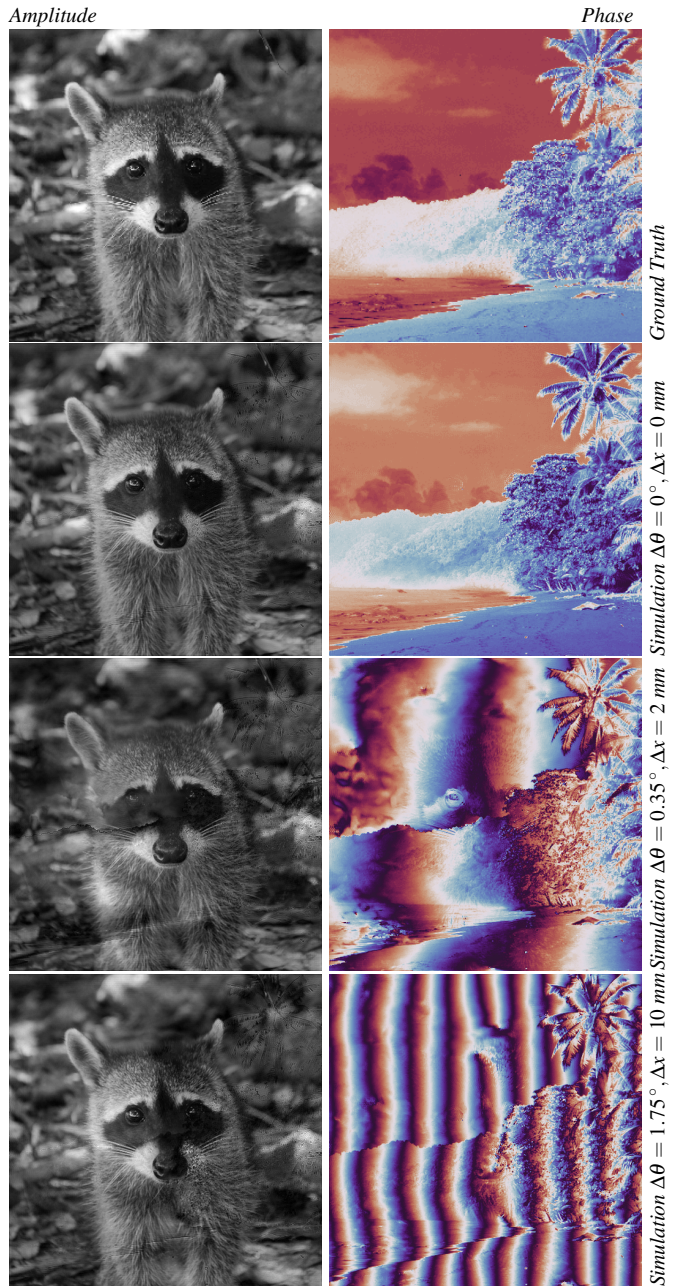*Amplitude*   *Phase*

Figure 6: Demonstrating the impact of misalignment of the whole LED panel on reconstruction amplitude (left) and phase (right) in respect to ground truth (top). Even a misalignment of mere $0.35°$ (2mm shift) renders the recovered phase quite useless.

As an example for such a case, the order of magnitude of the calibrated misalignment, $\mathcal{O}(\Delta x_n) = \log_{10}(\Delta x_n)$, is shown in Figure 7 for all bright-field LEDs.
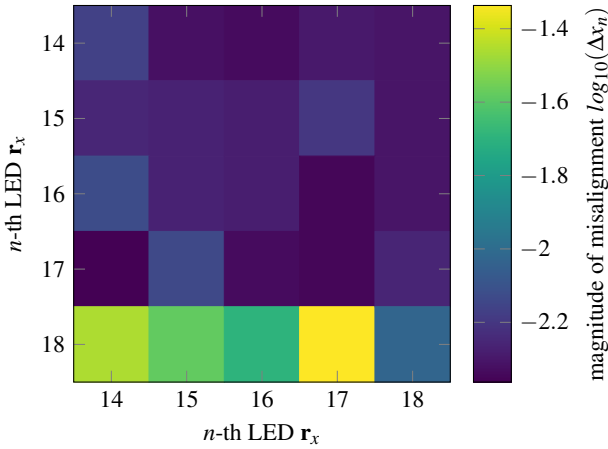

Figure 7: *Order of magnitude of the position misalignment for the bright field region of the LED panel.*

One can clearly see, that the majority of the values are quite in the same range, except those in the bottom row, where they are far off (roughly one order of magnitude). Though the explanation for this is not obvious, but may be neared with a cautious look at the spectra in question. It turns out, that due to the misalignment of $\Delta x = -5$ mm, $\Delta y = 8$ mm, the bottom row LEDs are shifted just outside the cutoff frequency, thus into the dark-field!

It is a hard prerequisite for the proposed calibration though, that the images are taken under bright field conditions, so these values are not to be considered. But how to find out if the given image was indeed a bright field image, thus the calibration result could be considered significant?

A first estimation of the corrections significance conveniently comes included in the procedure `imfindcircles`: the *strength* of the found circles; sort of the probability, that the found circle is indeed a circle.

It appears, that the results with a strength below the order $\mathcal{O}(-2)$ are probably not significant anymore, and may be rendered outliers. To visualise this, the initial and actual (shifted) grid is shown in Figure 8, together with the corrected positions (circles), colour-coded in order of magnitude of their strength.

The relation between the strengths and the validity of the corrections are quite evident, yet the precise border between in- and outliers is made empirically, and unfortunately have to be expected to vary with respect to the sample in question!

Yaw

A considerably harder problem is the case, where the LED panel is turned around the z-axis: Yaw. Like shift it is not that easy to align in a physical calibration step, as one has to lower the focus down to the LED panel. Additionally, yaw results in a misalignment that is proportional to the distance of the LED to the centre of the panel, rendering previously used descriptive statistics of the whole panel as one ensemble, including state of the art correction methods [2], useless.

The solution proposed here is to fit the set of corrected positions to a grid, and subsequently to evaluate the angle γ between
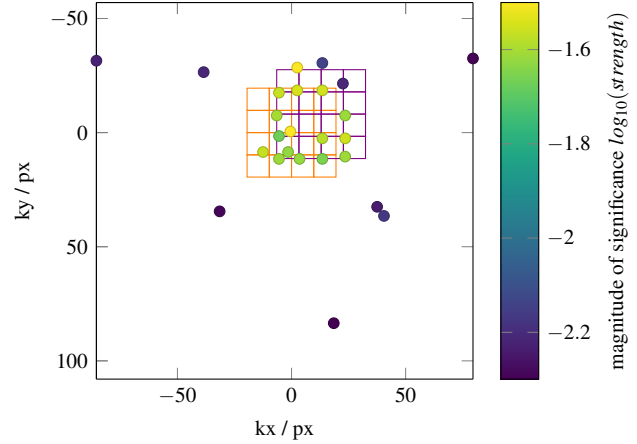

Figure 8: *Correcting shift: Comparison of the k-space projections $\mathbf{k}_n$ (nodes) of the bright field LED positions of the slightly shifted panel (violet); versus the initially assumed grid (orange); versus the corrected positions (circles), colour-coded in the order of magnitude of their strengths (colour, higher is better).*

this and the initial grid for each row and each column separately:

$$\gamma \approx \arctan(\beta) \tag{4}$$

where β refers to the slope of the *horizontal* and *vertical* lines of the grid in respect to the initial grid. In the horizontal case, ζ denotes the kx-axis, and χ denotes the ky-axis; in the vertical case vice versa. Since the data points of these lines have to be considered noisy, we assume a linear progression, via solving the least squares fit:

$$\zeta = \beta \chi + \delta \tag{5}$$

Depending on the size of the bright-field area of $n_b \times n_b$ LEDs, we end up with n_b horizontal inclinations γ_x and n_b vertical ones γ_y, which can be considered one statistical ensemble each. Again, careful observation of the deviations reveals if the panel is yawed (low deviations) or otherwise skewed (high deviations); And thus if we can deduce a meaningful mean and median.

Finally this allows the following conclusion: if—and only if—the both inclinations γ_x and γ_y are almost equal, we may deduce that this grid was only yawed. All other inclinations (e.g. pitch or roll) would have tilted the grid in a way, such that $\gamma_x \neq \gamma_y$. As an example, the bright-field area of the k-space grid of a slightly misaligned panel ($\gamma = 11°$) is shown in comparison with the actual and initial grids in Figure 9.

Roll & Pitch

The methods described so far provide a direct measure of the shift, respective yaw in the k-space grid of the LED panel, both of which are translation invariant in z-direction. Unfortunately these are the special cases of a bijection; where the misaligned LED panel is still strictly parallel to the object (and sensor), so it has a direct relation to the 2d grid in k-space.

Considering pitch and roll (rotations around the x-, respective the y-axis), the LED panel is not parallel to the sensor anymore. This results in a much harder problem: The mapping between the 3d real space and the measured 2d k-space is not bijective anymore. Thus it does not have an inverse function; it is not
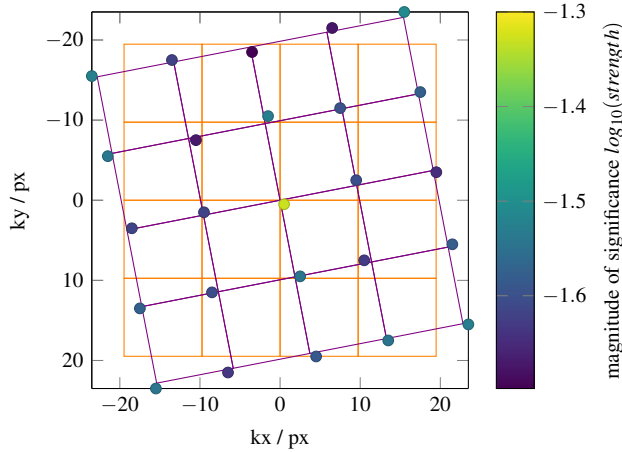
Figure 9: Correcting yaw: Comparison of the k-space projections $\mathbf{k}_n$ (nodes) of the corrected bf LED positions of the highly misaligned panel of Simulation 5 (circles), colour-coded in the order of magnitude of their strengths (fill, higher is better); versus the actual grid with yaw $\gamma = 11°$ (violet); versus initially assumed grid (orange).

possible to infer to the 3d real space misalignment by measurement of the 2d k-space grid!

An example for such a heavily tilted LED panel is shown in Figure 10: roll $\rho = 30°$, no pitch. The grid is still rectangular, but unlike previous examples the kx-, and ky-axis are not spaced equidistantly anymore! On the one hand the grid is *compressed* in ky-axis; one the other hand it forms a trapezoid. This is only very slightly visible in both shown examples, due to the panel being much farther away (327 mm in z-direction) as opposed to the difference in height caused by the tilt (±45 mm in z-direction).
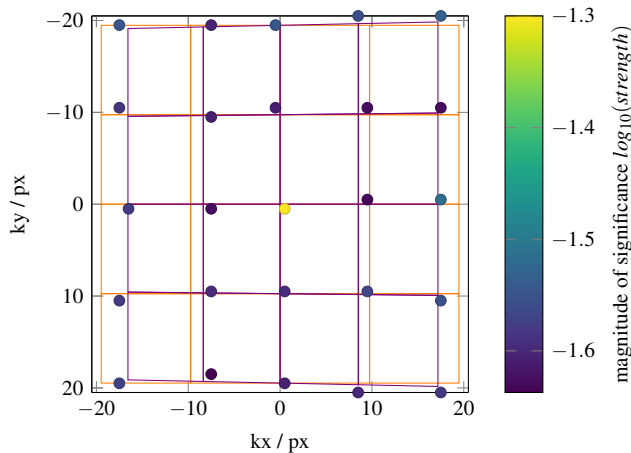

Figure 10: Correcting roll & pitch: Comparison of the k-space projections $\mathbf{k}_n$ (nodes) of the corrected bf LED positions of the highly misaligned panel of Simulation 6 (circles), colour-coded in the order of magnitude of their strengths (colour, higher is better); versus the actual grid with roll $\rho = 30°$ (violet); versus initially assumed grid (orange);

Unsurprisingly the resulting mean γ_x and γ_y values are both around zero, but with huge standard deviations. The mean is proffered here, because we do not have to consider extreme outliers

shifted into dark field. Either way, the spread of the values due to the compression & trapezoid effects is quite high—which is a strong indicator that the setup exceeds correctability.

An example of such a profoundly tilted LED panel—roll $\rho = 21°$ and pitch $\psi = 30°$— is shown in Figure 11. Evidently, the grid is not rectangular anymore. Analysis correctly depicts this: γ_x and γ_y values are both around zero for the kx-axis, yet around $10°$ for the ky-axis. Both median and mean deviations support this claim, which inherently points to tilt of the panel in x- and or y-axis.
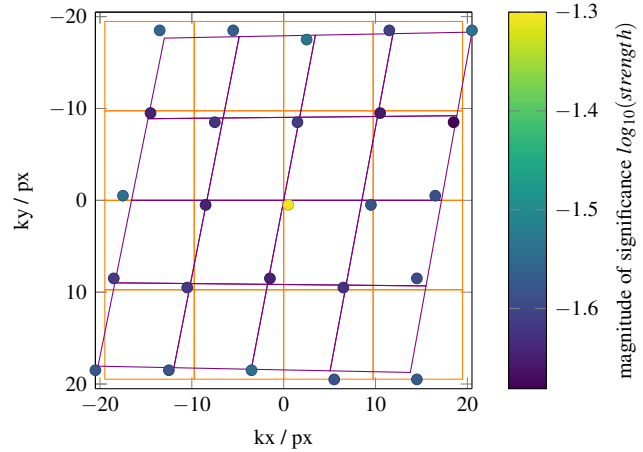

Figure 11: Correcting roll & pitch: Comparison of the k-space projections $\mathbf{k}_n$ (nodes) of the corrected bf LED positions of the highly misaligned panel of Simulation 6 (circles), colour-coded in the order of magnitude of their strengths (colour, higher is better); versus the actual grid with roll $\rho = 21°$ and pitch $p = 30°$ (violet); versus initially assumed grid (orange).

Table 1: Robustness of FPM to misalignment for all six degrees of freedom; empirical limits, indication and correction feasibility.

Parameter	Limit	Indication	Correction
Shift $\Delta\theta_x$	0.2°	low spread $\Delta\theta_x$	quantitative
Shift $\Delta\theta_y$	0.2°	low spread $\Delta\theta_y$	quantitative
Shift Δz	2%	high spread $\Delta\theta_x$, $\Delta\theta_y$	qualitative
Roll ρ	3°	$\gamma_x \neq \gamma_y$	qualitative
Pitch ψ	3°	$\gamma_x \neq \gamma_y$	qualitative
Yaw γ	2°	$\gamma_x \approx \gamma_y$	quantitative

Robustness, Indication & Correction Limits

The proposed methods enable the direct study of the impact, misalignment of the illumination source has on FPM recovery, shining light on which system parameters are more critical than others. Our calibration procedures permit precise correction of the experimental setup, where possible. Additionally the stated analysis allows assessment of present misalignment, even if uncorrectable by known methods. Since FPM is a very ill-posed problem, the reconstruction of the phase heavily depends on the object itself, so it is not possible to give a strict limit where

misalignment breaks the algorithm. Nevertheless we might name empirical limits based upon our simulations, up to which degree of misalignment the recovery still works. Empirical limits of misalignment for conventional FPM, indicators of the respective misalignment, and the feasibility of quantitative correction are shown in Table 1 for all six degrees of freedom. To our knowledge, such an analysis was never demonstrated before.

References

[1] Octave forge, image, function imfindcircles; https://octave.sourceforge.io/image/function/imfindcircles.html.

[2] R. Eckert, Z. F. Phillips, and L. Waller. Efficient illumination angle self-calibration in fourier ptychography. *Appl. Opt.*, 57(19):5434–5442, Jul 2018.

[3] J. R. Fienup. Phase retrieval algorithms: a comparison. *Appl. Opt.*, 21(15):2758–2769, Aug 1982.

[4] R. W. Gerchberg and W. O. Saxton. A practical algorithm for the determination of the phase from image and diffraction plane pictures. *Optik*, 35(2):237, 1972.

[5] X. Ou, R. Horstmeyer, C. Yang, and G. Zheng. Quantitative phase imaging via fourier ptychographic microscopy. *Opt. Lett.*, 38(22):4845–4848, Nov 2013.

[6] J. Sun, C. Zuo, J. Zhang, Y. Fan, and Q. Chen. High-speed fourier ptychographic microscopy based on programmable annular illuminations. *Scientific Reports*, 8(1):7669, May 2018.

[7] Wikipedia. Optical setup for fourier ptychography, 2018.

[8] L.-H. Yeh, J. Dong, J. Zhong, L. Tian, M. Chen, G. Tang, M. Soltanolkotabi, and L. Waller. Experimental robustness of fourier ptychography phase retrieval algorithms. *Opt. Express*, 23(26):33214–33240, Dec 2015.

Author Biography

Moritz Siegel received his BSc in Physics (2015) at the Graz University of Technology, Austria. He currently writes his master thesis (2020) at the Technische Universität (TU Wien) in cooperation with the Austrian Institute of Technology, about Fourier Ptychographic approaches to super-resolution; specialising in numerical physics, and experimental wave optics.

FH-Prof. DI Dr. Lukas Traxler earned his masters degree in Biomedical Engineering (2014) and a PhD degree in Technical Physics (2018), both at TU Wien, Austria. He joined the Austrian Institute of Technology (AIT) as scientist in 2017 at the Center for Vision, Automation & Control. Since 2014 he is lecturer at the University of Applied Sciences Technikum Wien, where he earned the Fachhochschulprofessor (FH-Prof.) in 2019. His main research areas are technical optics and computational imaging.

DI Laurin Ginner PhD wrote his doctoral thesis on the Medical University of Vienna (2019) after completing his master thesis in Physical Energy and Measurement Engineering at TU Wien. He joined the Austrian Institute of Technology (AIT) in March 2020 as a Scientists in the topics technical optics and computational imaging. The PhD Thesis was: Advanced techniques for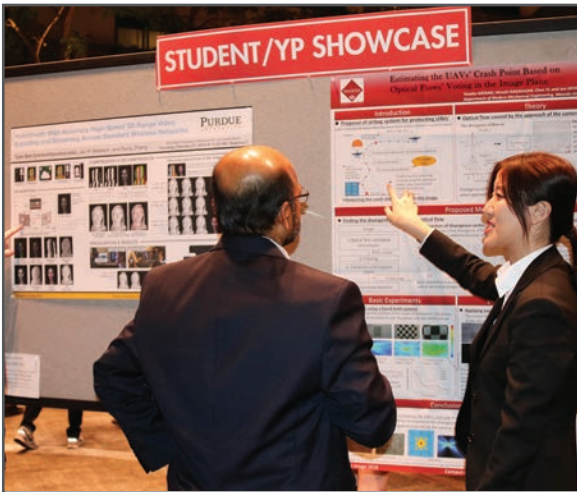 functional parallel optical coherence tomography.